(Received 15 April 2026, Accepted 28 May 2026, Scheduled 9 July 2026)

Pattern Synthesis for Sparse Linear Arrays by Employing a Partitioning Optimization Strategy Based on Differential Evolution

Jinyi Yang, Xinkuan Wang*, Chenxin Qi, Ping Wang, Lei Wang, Linjun Zhao, and Zhaoxin Xiong

School of Physics and Telecommunication Engineering, Shaanxi University of Technology, Hanzhong 723000, Shaanxi, China

ABSTRACT: A partition optimization strategy (POS) based on the differential evolution (DE) algorithm is proposed for low sidelobe synthesis of sparse linear arrays (SLAs). The approach starts by dividing the array aperture into a centrally symmetric full zone and several sparse subzones, where elements are fully arranged in the former zone and sparsely populated in other zones. Then, by introducing random parameters, including a full-zone adjustment factor, sparse subzone reduction factors, and sparse subzone filling factors, both the size of the full zone and the array aperture, as well as the total number of elements, could be dynamically adjusted. Next, for each sparse subzone, two random parameters are introduced to generate a nonuniform vector based on the 1D Rastrigin function so that the elements within the current zone are non-uniformly arranged by using the components of the vector. Finally, all the aforementioned parameters were optimized by the DE algorithm to find the SLA with reduced sidelobe level. Numerical simulations demonstrate that this method can reduce the SLAs' sidelobe level by 0.37∼4.34 dB along with the decrement of the number of elements by about 0.7%–15.0%, compared to the published reports.

1. INTRODUCTION

Sparse array (SA) refers to an array configuration in which the elements are randomly distributed within the aperture. It helps reduce system weight, hardware cost, and element mutual coupling by using SAs, thereby finding applications in fields such as radar detection, satellite communication, and radio astronomy [1–3]. Over the past few decades, extensive research has been conducted in the pattern synthesis of sparse arrays. Commonly used algorithms include heuristic optimization algorithms (HOAs), such as ant colony optimization (ACO) [4], genetic algorithm (GA) [5], and differential evolution (DE) [6, 7], as well as some hybrid algorithms that integrate with HOAs [8–12]. Moreover, other methods, such as almost difference set (ADS) algorithms [13, 14], iterative Fourier technique (IFT) [15, 16], iterative chirp-z transform technique (ICZT) [17], matrix mapping method [18, 19], and Bayesian compressive sampling (BCS) [20, 21], have also been proposed.

To the best of our knowledge, although the aforementioned methodologies have shown good performance in the pattern synthesis of different types of SAs, most of them require the total number of elements and aperture size to be predetermined. The operation is not conducive to improving the performance indexes of sparse arrays with the minimum number of elements and the best aperture size. To address this issue, Wang et al. [12] proposed a new strategy named partial density tapering (PDT) for the synthesis of sparse planar arrays. According to PDT, the 2D aperture is divided into a series of concentric loops that have the same shape as the aperture, and the elements could only be equipped on these loops. Further, the loops near the center of the array are fully populated, whereas the peripheral loops far from the center are sparsely arranged. Consequently, the number of elements to be optimized is significantly reduced, and the element layout always maintains a density-tapering distribution. For the aforementioned reasons, this strategy not only greatly reduces the computational burden of the HOA, but also effectively avoids infeasible solutions.

In this paper, inspired by the method in [12], we propose a partition optimization strategy based on differential evolution (POSDE) for the low-sidelobe synthesis of sparse linear array (SLA). Firstly, the array aperture is divided into a centrally symmetric full zone and a certain number of sparse subzones (SSZs). In the full zone, the elements are fully arranged, whereas in SSZs, they are sparsely equipped. Then, by introducing random parameters, such as a full zone adjustment factor and a sparse subzone reduction factor, the dimensions of both the full and sparse zones are simultaneously reduced, thereby achieving a reduction in the overall array aperture size. Further, a set of filling factors that describe the number of elements accommodated in all SSZs is introduced so that the total number of elements in SLA can be dynamically adjusted via optimizing the filling factors between fixed upper and lower bounds. Moreover, in order to arrange the elements in SSZs, two random parameters are introduced for each SSZ to generate a uniform vector. Then, the vector is mapped to a nonuniform vector by using the 1D Rastrigin function, and the elements of

* Corresponding author: Xinkuan Wang (wxkuan@snut.edu.cn).

the SSZ are non-uniformly arranged by using components of the latest vector.

Finally, all the aforementioned parameters are optimized by the DE algorithm to find the best design with reduced sidelobe level. Some numerical results for different SLAs are presented and compared with the published reports to demonstrate the effectiveness of the proposed method.

The paper is organized as follows. Section 2 describes the formulation of the POSDE. Section 3 provides several numerical examples to validate its performance, and Section 4 concludes the work.

2. FORMULATION OF THE PROPOSED METHOD

Assume a linear array consisting of N isophoric elements placed along the x-axis. The pattern of the array can be expressed as

$$F(u) = \sum_{n=0}^{N-1} A_n e^{jkux_n} \tag{1}$$

where k is the wavenumber; $u = \sin\theta$; θ is the angle between the far-field direction and the array normal; A_n and x_n represent the excitation and coordinate position of the n^{th} element, respectively. Furthermore, we assume that the elements are fed with equal amplitudes, thus, A_n can be regarded as 1.

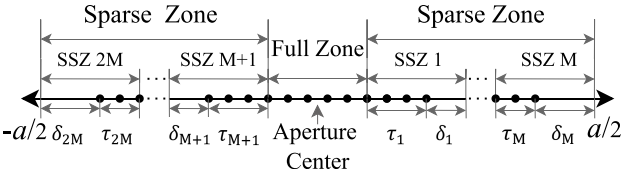

FIGURE 1. Schematic diagram of aperture division for sparse linear array.

Considering a linear array with the initial aperture length equal to a (the unit is λ, which stands for a wavelength, and the same applies hereafter), we divide the aperture into three zones: a full zone and two sparse zones. All zones are symmetrical with the aperture center as the reference point, as shown in Figure 1. If we denote the minimum value of element spacing as d, then the full zone means that the elements are uniformly populated with spacing d, while the sparse zone corresponds to the configuration in which the elements are randomly arranged with element intervals greater than d. To determine the size of the full zone, we define ε as the full zone adjustment factor. Therefore, the initial length of the full zone is

$$b = a \cdot \varepsilon, \quad \text{for } \varepsilon \in [0.2, 0.6] \tag{2}$$

Accordingly, the number of elements that can be accommodated in the full zone is expressed by

$$G = 2 \cdot \text{int}(0.5 \cdot b/d) \tag{3}$$

where G is an even number, and $\text{int}(A)$ denotes the nearest integer less than or equal to A. The element positions within the full zone are recorded as

$$x_{\pm g} = \pm(g - 0.5) \cdot d, \quad \text{for } g = 1, 2, \cdots, G/2 \tag{4}$$

According to Eq. (4), the coordinates of the element locations on the left and right edges of the full zone can be denoted as

$$x_{\pm G/2} = \pm(G/2 - 0.5) \cdot d \tag{5}$$

Hence, the actual length of the full zone is

$$b' = 2 \cdot (G/2 - 0.5) \cdot d \tag{6}$$

By comparing (2) and (6), it can be seen that $b \geq b'$. In other words, the actual length of the full zone was somewhat reduced compared to its initial value. Therefore, the lengths of the two sparse zones beside the full zone shown in Figure 1 are both

$$\eta = (a - b')/2 \tag{7}$$

Furthermore, both the sparse zones are divided into M SSZs of equal length. As a result, a total of $2M$ SSZs were generated, and we numbered them sequentially from 1 to $2M$, as shown in Figure 1. The length of an individual SSZ is

$$l = \eta/M \tag{8}$$

Correspondingly, the maximum number of elements that can be populated in an SSZ is:

$$t = \text{int}(l/d) \tag{9}$$

To determine the number of elements in the SSZ, we define the filling factor as the ratio of the actual number of elements in the SSZ to the number of elements when the SSZ is fully populated. Then, a vector constituted by the filling factors of all SSZs is introduced and described as

$$\mathbf{f} = [f_1, f_2, \cdots, f_M, f_{M+1}, \cdots, f_{2M}] \tag{10}$$

where the component $f_m, m = 1, 2, ...2M$ represents the filling factor of m^{th} SSZ. Further, let f_m be varied within the specified upper and lower bounds; thus, we have

$$f^{\min} \leq f_m \leq f^{\max}, \quad \text{for } m = 1, 2, \cdots, 2M \tag{11}$$

Accordingly, the number of elements accommodated in m^{th} SSZ is

$$q_m = \text{floor}(t \cdot f_m), \quad \text{for } m = 1, 2, \cdots, 2M \tag{12}$$

To illustrate the method for reducing the aperture size, we consider the m^{th} SSZ as an example. First, place all the elements within the current SSZ from left to right with an interval of d; thus, the initial positions of those elements can be described by the vector

$$\mathbf{X}_m^0 = \begin{cases} \frac{b'}{2} + (m-1) \cdot l + \gamma \cdot d, & \text{for } m \leq M \\ -\left[\frac{b'}{2} + (m - M - 1) \cdot l + \gamma \cdot d\right], & \text{else} \end{cases} \tag{13}$$

where $\boldsymbol{\gamma}$ represents the vector $\{1, 2, \cdots, q_m\}$. For convenience, the size occupied by these elements is denoted as $\tau_m = q_m \cdot d$. Therefore, the residue of the m^{th} SSZ, which describes the unoccupied part of the current zone, can be expressed as

$$\delta_m = l - \tau_m \tag{14}$$

Figure 1 shows the schematic diagram of aperture division for SLA and describes the difference between τ_m and δ_m, where the symbols "•" denote the elements. Further, a reduction factor $\sigma_m \in (0, 1)$ is introduced to reduce the length of δ_m, and

thereby the residue of m^{th} SSZ is updated as

$$\delta'_m = \delta_m \cdot \sigma_m, \quad \text{for } m = 1, 2, \cdots, 2M \tag{15}$$

According to (14), the length of m^{th} SSZ is reduced to

$$l'_m = \delta'_m + \tau_m \tag{16}$$

Hence, the element locations described by (13) are updated to the vector

$$\mathbf{X}_m^1 = \begin{cases} \frac{b'}{2} + \boldsymbol{\gamma} \cdot d, \text{ for } m = 1 \\ \frac{b'}{2} + \sum_{h=1}^{m-1} l'_h + \boldsymbol{\gamma} \cdot d, \text{ for } 2 \le m \le M \\ -\left[\frac{b'}{2} + \boldsymbol{\gamma} \cdot d\right], \text{ for } m = M+1 \\ -\left[\frac{b'}{2} + \sum_{h=M+1}^{m-1} l'_h + \boldsymbol{\gamma} \cdot d\right], \text{ for } M+2 \le m \le 2M \end{cases} \tag{17}$$

After all SSZs are reduced according to Eqs. (15)–(17), they are connected end to end to compress the overall aperture of the SLA.

Since the arrangement of elements in SSZs described by (17) is not conducive to suppressing the sidelobe level of SLA, it is necessary to find a strategy that enables a nonuniform distribution of elements within the SSZ to suppress the array's sidelobe level. However, to realize a random element arrangement in SSZ, it is usually necessary to introduce the same number of random variables as the number of elements in the current SSZ. Consequently, the lengths of different individuals to be optimized are inconsistent, which makes intelligent optimization algorithms unusable. For this reason, two random variables are introduced for each SSZ to realize a nonuniform arrangement of the elements using the 1D Rastrigin function. For a detailed illustration, we still consider the m^{th} SSZ as an example. The function of 1D Rastrigin can be expressed as

$$v(x) = x^2 - 10\cos(2\pi x) + 10 \tag{18}$$

with $x \in (-\infty, +\infty)$. Figure 2 describes the variation curve of the function within the interval $(-4, 4)$. Firstly, two random parameters, labeled as ϑ_m and ξ_m, are generated in between the interval $(-4, 4)$ with $\vartheta_m < \xi_m$. Then, a uniformly distributed vector is generated and recorded as

$$\mathbf{y}_m = \text{lins}\left(\vartheta_m, \xi_m, q_m\right) \tag{19}$$

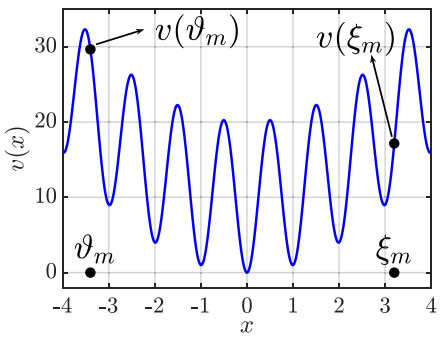

FIGURE 2. Diagram of 1D Rastrigin function.

Eq. (19) describes a set of coordinate points that are evenly spaced along the x-axis from ϑ_m to ξ_m, and the total number of points is q_m. Then, the vector $\mathbf{y}_m$ is mapped to a nonuniform vector by substituting it into (18); thus, we obtain a new vector

$$\mathbf{V}_m = v(\mathbf{y}_m) \tag{20}$$

Next, with the components of $\mathbf{V}_m$, the residue δ'_m is divided into q_m unequal parts, which can be expressed by the vector

$$\boldsymbol{\Delta}\mathbf{V}_m = \frac{\delta'_m \cdot \text{cumsum}(\mathbf{V}_m)}{\text{sum}(\mathbf{V}_m)} \tag{21}$$

where $\text{sum}(\cdot)$ and $\text{cumsum}(\cdot)$ represent the summation and cumulative summation of the components in vector $\mathbf{V}_m$, respectively. The components in vector $\boldsymbol{\Delta}\mathbf{V}_m$ represent the increments of the element positions of the m^{th} SSZ, in order from left to right. Therefore, by assigning $\boldsymbol{\Delta}\mathbf{V}_m$ to (17), the latest element coordinates of the m^{th} SSZ are updated as

$$\mathbf{X}_m^2 = \begin{cases} \frac{b'}{2} + \boldsymbol{\gamma} \cdot d + \boldsymbol{\Delta}\mathbf{V}_m, \text{ for } m = 1 \\ \frac{b'}{2} + \sum_{h=1}^{m-1} l'_h + \boldsymbol{\gamma} \cdot d + \boldsymbol{\Delta}\mathbf{V}_m, \text{ for } 2 \le m \le M \\ -\left[\frac{b'}{2} + \boldsymbol{\gamma} \cdot d + \boldsymbol{\Delta}\mathbf{V}_m\right], \text{ for } m = M+1 \\ -\left[\frac{b'}{2} + \sum_{h=M+1}^{m-1} l'_h + \boldsymbol{\gamma} \cdot d + \boldsymbol{\Delta}\mathbf{V}_m\right], \\ \quad \text{for } M+2 \le m \le 2M \end{cases} \tag{22}$$

Because the 1D Rastrigin function is non-periodic and exhibits high-frequency oscillations, its values are extremely sensitive to small changes in the independent variable. This sensitivity leads to large fluctuations in the function value over any random interval, which, in turn, causes the element locations in the m^{th} SZZ determined by (22) to exhibit greater randomness. As a result, the element positions described by Eq. (22) are non-uniformly distributed, which is conducive to suppressing the sidelobe level of SLA.

By applying the procedures described in (13)–(22) to all sparse subzones, a random distribution of elements is achieved in all SSZs. Additionally, because each SSZ requires only two random variables to control the element layout within the same partition, heuristic algorithms can be used so that the lengths of different individuals remain consistent during the optimization process. Based on the above analysis, the parameters involved in the aforementioned procedures, such as the full zone adjustment factor ε, minimum element spacing d, filling factors of all SSZs, and reduction factors, are combined to form the individual vector as

$$\begin{aligned} \mathbf{X} = \{&\varepsilon, d, f_1, f_2, \cdots, f_{2M}, \sigma_1, \sigma_2, \cdots, \sigma_{2M}, \vartheta_1, \vartheta_2, \cdots, \\ &\vartheta_{2M}, \xi_1, \xi_2, \cdots, \xi_{2M}\} \end{aligned} \tag{23}$$

where d belongs to $[0.5\lambda, 0.55\lambda]$. Finally, the individual is optimized by employing the differential evolution algorithm to suppress the sidelobe level of SLA.

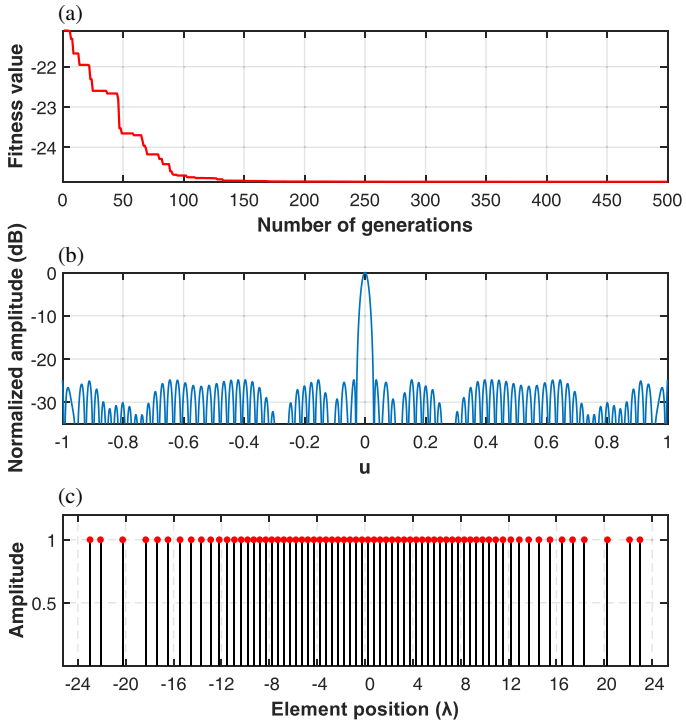

FIGURE 3. Synthesis for symmetrical SLA with an aperture length of 45.96λ. (a) The convergence curve of the fitness value, (b) the far-field pattern, and (c) the distribution of element locations.

3. NUMERICAL EXAMPLES

To illustrate the effectiveness of the proposed method, some numerical instances for SLA of different sizes are presented and compared with published reports. The population size was set to 100, and the number of evolutions was 500. Unless otherwise specified, the filling factors of all SSZs are constrained within the range (0.3, 0.8).

3.1. Symmetrical Sparse Linear Array

Considering a symmetrical SLA with an initial aperture length of 49.5λ, we set the number of SSZs equal to 4. However, because the array is symmetrical about its center, only two SSZs are independent. By using this method, an SLA with a sidelobe level of -24.86 dB and a 3 dB beamwidth equal to 1.318 degrees was created. The convergence curve in Figure 3(a) depicts the fitness value versus the number of generations, together with Figure 3(b) describing the far-field pattern of the best SLA. The effective aperture length, minimum element spacing, and total number of elements in this array were 45.96λ, 0.5027λ, and 68, respectively. Compared with algorithms such as ACO [4], IFT-DE [9], and the modified iterative Chirp-Z transform (MICZT) [17], the proposed method achieves the sidelobe reduction of 4.34 dB, 1.3 dB, and 3.99 dB, respectively. In addition, the aperture size is reduced by up to 3.54λ, whereas the number of elements is decreased by 10.5%–15%. Figure 3(c) shows the element distribution of the SLA, where the ordinate represents the normalized amplitude of the element excitations.

If the initial aperture length is increased to 99.5λ, we set the number of SSZs to 6. The SLA obtained by this method has an effective aperture length of 91.03λ. In addition, the sidelobe level is -26.71 dB, which shows sidelobe reduction of 1.84$\sim$3.85 dB with almost no sacrifice of beamwidth, as compared to reports of the novel binary differential evolution (NBDE) [6], differential evolution and lévy flight (DELF) [7], IFT-DE [9], IFT [15], probability tapering IFT (PTIFT) [16], and MICZT [17]. Nevertheless, the number of elements required by this array is 126, which is six less than that obtained by the other methods. Figures 4(a) and (b) show the convergence curve of this synthesis and the farfield pattern of the best SLA, respectively.

Furthermore, if we take the same initial parameters as in the previous instance but simply change the range of filling factors from (0.3, 0.8) to (0.4, 0.9), the radiation pattern of the obtained SLA is displayed in Figure 5. The array consists of 144 elements, with a sidelobe level of -25.82 dB and beamwidth of 0.602 degrees, while the aperture length remains almost unchanged. Compared to the results obtained by the M-cGA [5], NBDE [6], DELF [7], IFT-DE [9], hybrid genetic algorithm and modified IFT (HGAMIFT) [10], almost difference set–GA (ADSGA) [13], IFT [15], and MICZT [17], the number of elements is saved by 5.2%–6.4%, while the sidelobe levels are decreased by about 1.73–2.9 dB. Table 1 lists the coordinates of all elements in the array.

To assess the performance of the method for the synthesis of ultra-large SLA, the initial aperture length was increased to 999.5λ with the number of SSZs equal to 16. The obtained SLA has a sidelobe level of -36.70 dB, which is 3.65 dB lower than the result reported by DELF [7]. Moreover, the aperture length was reduced to 989.2λ, and the total number of elements was decreased by 12. Table 2 presents all the com-

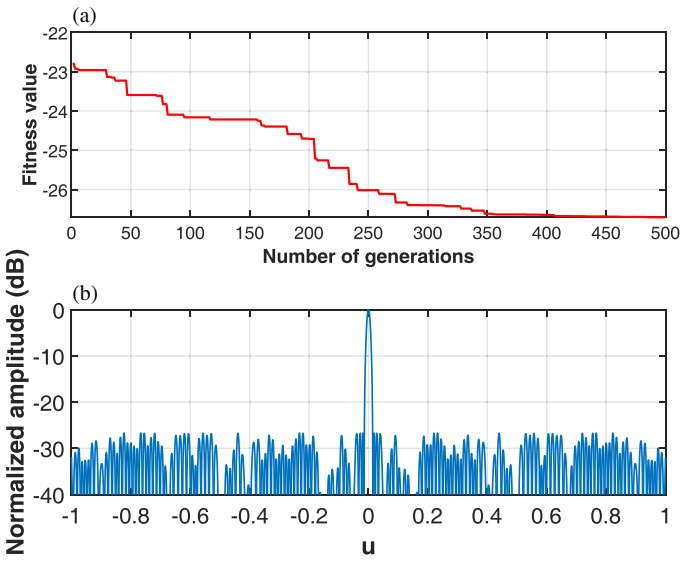

FIGURE 4. Synthesis for symmetrical SLA with an aperture length of 91.03λ. (a) The convergence curve of the fitness value and (b) the far-field pattern.

TABLE 1. The element coordinates of the symmetrical SLA with an aperture length of 99.44λ (unit: λ).

Element Number	Element Position	Element Number	Element Position	Element Number	Element Position
1,144	±0.25	25,120	±12.25	49,96	±26.3698
2,143	±0.75	26,119	±12.75	50,95	±27.1996
3,142	±1.25	27,118	±13.25	51,94	±28.0833
4,141	±1.75	28,117	±13.75	52,93	±28.9255
5,140	±2.25	29,116	±14.25	53,92	±29.9898
6,139	±2.75	30,115	±14.75	54,91	±30.7444
7,138	±3.25	31,114	±15.25	55,90	±31.6590
8,137	±3.75	32,113	±15.75	56,89	±32.3776
9,136	±4.25	33,112	±16.25	57,88	±33.1860
10,135	±4.75	34,111	±16.75	58,87	±33.9183
11,134	±5.25	35,110	±17.25	59,86	±34.6657
12,133	±5.75	36,109	±17.9644	60,85	±35.4596
13,132	±6.25	37,108	±18.5531	61,84	±36.1934
14,131	±6.75	38,107	±19.0614	62,83	±37.0946
15,130	±7.25	39,106	±19.5776	63,82	±37.8639
16,129	±7.75	40,105	±20.1856	64,81	±38.9166
17,128	±8.25	41,104	±20.9205	65,80	±40.9655
18,127	±8.75	42,103	±21.7505	66,79	±41.7819
19,126	±9.25	43102	±22.5937	67,78	±43.7012
20,125	±9.75	44,101	±23.3623	68,77	±44.9803
21,124	±10.25	45,100	±24.0095	69,76	±45.6235
22,123	±10.75	46,99	±24.5550	70,75	±47.5624
23,122	±11.25	47,98	±25.0746	71,74	±48.6083
24,121	±11.75	48,97	±25.6598	72,73	±49.7179

parison results between POSDE and some existing algorithms, where N, BW, and SLL denote the total number of elements, 3 dB beamwidth, and sidelobe level, respectively. The findings demonstrate that relative to other approaches, the symmetrical SLAs yielded by the proposed method could reduce the sidelobe levels by 0.37–4.34 dB and decrease the number of elements by 0.7–15%. Nevertheless, the aperture length has been decreased by 10.3λ at most.

TABLE 2. Comparative synthesizing results for symmetrical SLAs by using the POSDE and some published tools.

Aperture length (λ)	Methods	N	SLL (dB)	BW (°)
49.50	ACO [4]	80	−20.52	-
49.50	IFT-DE [9]	76	−23.56	-
47.50	MICZT [17]	76	−20.87	1.231
45.96	POSDE	68	−24.86	1.318
73.00	NBDE [6]	78	−19.51	-
73.00	DELF [7]	78	−20.59	-
69.73	POSDE	76	−21.07	1.003
90.50	NBDE [6]	132	−23.03	-
90.50	DELF [7]	132	−24.87	-
93.00	IFT [15]	132	−22.86	0.685
92.00	PTIFT [16]	132	−23.3	0.687
97.00	MICZT [17]	132	−23.28	0.672
99.50	IFT-DE [9]	132	−24.59	0.680
91.03	POSDE	126	−26.71	0.688
99.50	M-cGA [5]	154	−23.75	-
98.50	NBDE [6]	152	−23.31	-
98.50	DELF [7]	152	−24.09	-
99.50	IFT-DE [9]	154	−24.04	0.580
99.50	HGAMIFT [10]	154	−23.47	-
98.50	ADSGA [13]	154	−23.05	-
99.50	IFT [15]	154	−22.92	0.588
99.50	MICZT [17]	154	−23.1	0.560
99.44	POSDE	144	−25.82	0.602
250.50	DELF [7]	251	−22.69	-
250.50	ADSGA [13]	251	−21.31	-
242.87	POSDE	248	−23.06	0.286
999.50	DELF [7]	1540	−33.05	-
989.20	POSDE	1528	−36.70	0.057

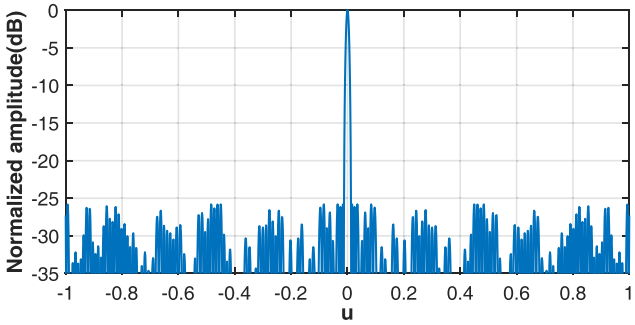

FIGURE 5. The far-field pattern for the symmetric SLA with an aperture length of 99.44λ.

3.2. Asymmetrical Sparse Linear Array

For the asymmetric SLA, we still set the initial length of the array to 49.5λ and the number of SSZs to four. Unlike the symmetrical SLA, all the SSZs here are independent; thus, the number of variables to be optimized is nearly twice as much as in the symmetric case. The convergence curve obtained by performing the POSDE is depicted in Figure 6(a), which indicates that the best fitness value is reached at the 450$^{\text{th}}$ generation. The obtained SLA comprises 67 elements, exhibiting a sidelobe level of −25.61 dB, a beamwidth of 1.289 degrees, and an aperture length of 47.13λ. Compared to the symmetrical counterpart, the number of elements is reduced by one, while the sidelobe level and beamwidth are decreased by 0.75 dB and 0.029 degrees, respectively. Figure 6(b) depicts the SLA's radiation pattern, and the matchstick diagram in Figure 6(c) shows the distribution of elements across the aperture.

Similarly, for the SLA with initial aperture length equal to 99.5λ, the convergence curve using POSDE is presented in Figure 7(a), while Figure 7(b) depicts the radiation pattern of the best SLA. The array consists of 133 elements, which has a sidelobe level of −26.98 dB, a beamwidth of 0.659 degrees, and its aperture length is reduced to 97.09λ. Compared to those obtained by NBDE [7], IFT-DE [9], IFT [15], PTIFT [16], and MICZT [17], the number of elements is reduced by six, and the sidelobe level is lowered by 1.52∼2.68 dB. Table 3 tabulates all the comparative results of POSDE with existing approaches.

3.3. Sensitivity Analysis for the Number of Sparse Subzones

A limitation of the proposed method is that the number of SSZs (denoted by Q) needs to be predetermined. The value of Q has

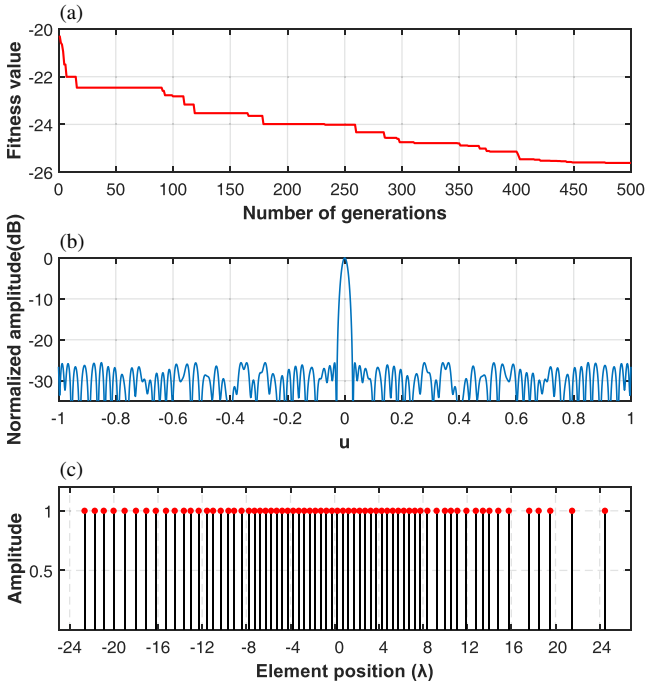

FIGURE 6. Synthesis for asymmetrical SLA with an aperture length of 47.13λ. (a) The convergence curve of the fitness value, (b) the far-field pattern, and (c) the distribution of element locations.

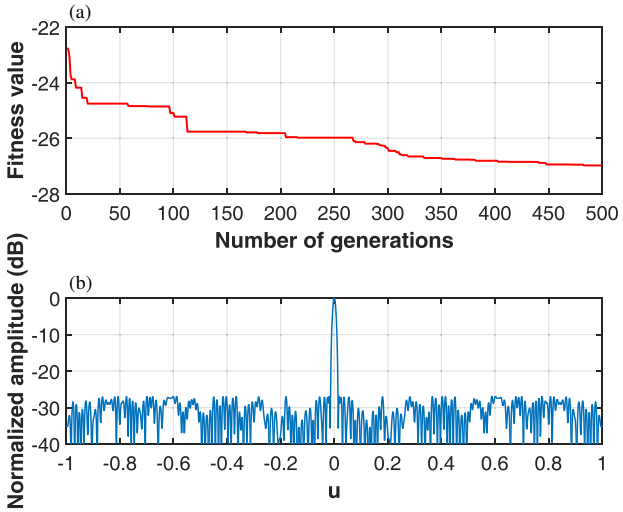

FIGURE 7. Synthesis for asymmetrical SLA with an aperture length of 97.09λ. (a) The convergence curve of the fitness value and (b) the far-field pattern.

an important impact on the optimization results. To address the issue, we take a symmetrical linear array with an aperture length of 49.5λ as an example and perform numerical simulations with Q equal to 4, 6, and 8, respectively. The convergence curves of the algorithm under different cases are shown in Figure 8. It can be seen that when $Q = 4$, the convergence speed is effectively accelerated. When the evolution generations reach 150, the algorithm almost converges to the optimal solution. When the evolution generations reach 500, the sidelobe level of the best array is reduced by 0.28 dB and 0.9 dB, respectively, compared to the results of the other two cases.

TABLE 3. Comparative synthesizing results for asymmetrical SLAs by using the POSDE and some published tools.

Aperture length (λ)	Methods	N	SLL (dB)	BW ($^\circ$)
47.13	POSDE	67	-25.61	1.289
96.00	NBDE [6]	139	-24.64	-
99.50	IFT-DE [9]	139	-25.46	0.640
99.00	IFT [15]	139	-24.30	0.643
99.50	PTIFT [16]	139	-24.70	0.642
99.50	MICZT [17]	139	-24.59	0.644
97.09	POSDE	133	-26.98	0.659

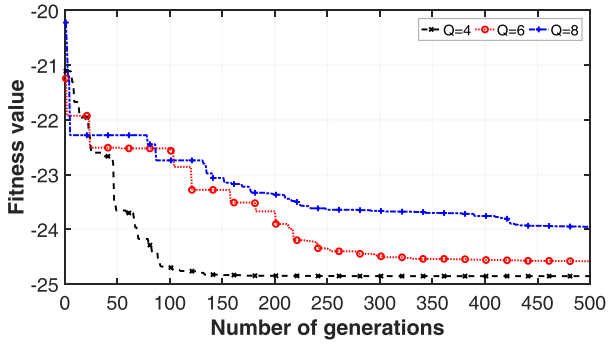

FIGURE 8. The convergence curves of fitness value versus the number of generations for $Q = 4$, 6, and 8, respectively (aperture length: 49.5λ).

Similarly, when the aperture of the array is increased to 99.5λ, the convergence curves of the algorithm for $Q = 4$, 6, and 8 are shown in Figure 9. We can see that the algorithm exhibits better performance for $Q = 6$. The sidelobe level of the SLA in this case is reduced by about 2.8 dB compared with the cases when $Q = 4$ and 8. Therefore, tthe algorithm performance is highly sensitive to the value of Q. In general, the appropriate value of Q needs to be determined through a small number of numerical experiments. However, through extensive prior numerical experiments, we suggest that it is a suitable way to increase the number of sparse subzones by 2$\sim$3 for each increment of 50λ in the aperture length.

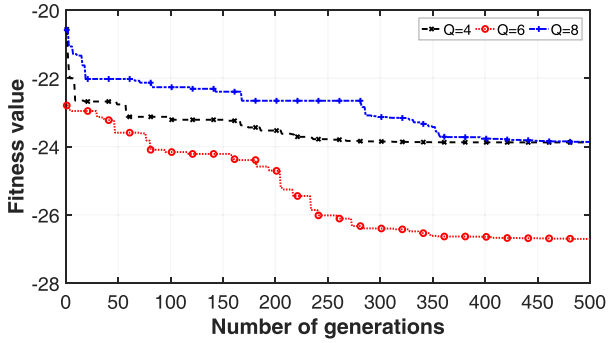

FIGURE 9. The convergence curves of fitness value versus the number of generations for $Q = 4$, 6, and 8, respectively (aperture length: 99.5λ).

4. CONCLUSION

For the low-sidelobe synthesis of sparse linear arrays, we propose a partition-based optimization strategy combined with a differential evolution algorithm. This approach overcomes the limitation of most algorithms that require the number of elements to be preset in advance, thus enabling dynamic optimization of both the total number of elements and the aperture length. Consequently, it is possible to obtain an SLA with the desired performance by equipping as few elements as possible with a reduced aperture size. Simulation results demonstrate that relative to existing algorithms, this method can reduce the sidelobe levels of SLA by approximately 0.37–4.34 dB and decrease the number of elements by 0.7%–15%. Meanwhile, the aperture lengths have also been somewhat reduced. All numerical results were obtained using a PC equipped with a 16-GB RAM and an Intel I5-12400 processor. The calculation time for different instances ranged from 2 to 14 minutes.

However, there are still some limitations of the method that need further investigation. Firstly, the number of sparse subzones needs to be preset through a few preliminary numerical experiments, which affects the acquisition of the optimal solution. If the number of sparse partitions can be included as an optimization variable, it would facilitate enhancing the performance of the sparse array. Secondly, for each sparse subzone, two random variables need to be introduced and mapped via a 1D Rastrigin function to obtain a random arrangement of elements within the current zone. However, the approach is not unique, and its performance directly affects the acquisition of the best SLA. Therefore, it remains an issue that requires further investigation to explore a better method for nonuniform element arrangement.

ACKNOWLEDGEMENT

This work was supported in part by the Intelligent Multi-source Autonomous Navigation Research Project under Grant No. 62388101, in part by the Natural Science Basic Research Program of Shaanxi Province under Grant No. 2024JC-YBMS-540, in part by the Key Scientific Research Program Funded by Education Department of Shaanxi Provincial Government under Grant No. 25JS025 and Grant No. 25JS026, in part by the Key Research and Development Program Projects of Shaanxi Province under Grant No. 2025CY-YBXM-122, in part by the Graduate Innovation Fund Project of Shaanxi University of Technology under Grant No. SLGYCX2512, in part by the Scientific Research Plan of Shaanxi University of Technology under Grant No. SLGSYS07, and in part by the doctoral research start-up project of Shaanxi University of Technology under Grant No. SLGBSRCQD2026020.

REFERENCES

[1] Alvarez-Folgueiras, M., J. A. Rodriguez-Gonzalez, and F. Ares-Pena, "High-performance uniformly excited linear and planar arrays based on linear semiarrays composed of subarrays with different uniform spacings," *IEEE Transactions on Antennas and Propagation*, Vol. 57, No. 12, 4002–4006, Dec. 2009.

[2] Bucci, O. M. and S. Perna, "A deterministic two dimensional density taper approach for fast design of uniform amplitude pencil beams arrays," *IEEE Transactions on Antennas and Propagation*, Vol. 59, No. 8, 2852–2861, Aug. 2011.

[3] Jiang, Y. and S. Zhang, "An innovative strategy for synthesis of uniformly weighted circular aperture antenna array based on the weighting density method," *IEEE Antennas and Wireless Propagation Letters*, Vol. 12, 725–728, 2013.

[4] Quevedo-Teruel, O. and E. Rajo-Iglesias, "Ant colony optimization in thinned array synthesis with minimum sidelobe level," *IEEE Antennas and Wireless Propagation Letters*, Vol. 5, 349–352, 2006.

[5] Ha, B. V., M. Mussetta, P. Pirinoli, and R. E. Zich, "Modified compact genetic algorithm for thinned array synthesis," *IEEE Antennas and Wireless Propagation Letters*, Vol. 15, 1105–1108, 2016.

[6] Goudos, S., "Antenna design using binary differential evolution: Application to discrete-valued design problems," *IEEE Antennas and Propagation Magazine*, Vol. 59, No. 1, 74–93, Feb. 2017.

[7] Dai, D., M. Yao, H. Ma, W. Jin, and F. Zhang, "An effective approach for the synthesis of uniformly excited large linear sparse array," *IEEE Antennas and Wireless Propagation Letters*, Vol. 17, No. 3, 377–380, Mar. 2018.

[8] Jiang, Y., S. Zhang, Q. Guo, and X. Luan, "A hybrid strategy based on weighting density and genetic algorithm for the synthesis of uniformly weighted concentric ring arrays," *IEEE Antennas and Wireless Propagation Letters*, Vol. 16, 186–189, 2016.

[9] Wang, X.-K. and G.-B. Wang, "A hybrid method based on the iterative Fourier transform and the differential evolution for pattern synthesis of sparse linear arrays," *International Journal of Antennas and Propagation*, Vol. 2018, No. 1, 6309192, 2018.

[10] Cui, C., W. T. Li, X. T. Ye, and X. W. Shi, "Hybrid genetic algorithm and modified iterative fourier transform algorithm for large thinned array synthesis," *IEEE Antennas and Wireless Propagation Letters*, Vol. 16, 2150–2154, 2017.

[11] Zhang, J., X. Mao, M. Zhang, J. Hirokawa, and Q. H. Liu, "Synthesis of thinned planar arrays based on precoded subarray structures," *IEEE Antennas and Wireless Propagation Letters*, Vol. 22, No. 1, 44–48, Jan. 2023.

[12] Wang, X.-K., G.-B. Wang, and L. Wang, "Pattern synthesis for different sparse planar arrays by a hybrid unconstrained-heuristic approach," *IEEE Antennas and Wireless Propagation Letters*, Vol. 22, No. 3, 631–635, Mar. 2023.

[13] Oliveri, G. and A. Massa, "Genetic algorithm (GA)-enhanced almost difference set (ADS)-based approach for array thinning," *IET Microwaves, Antennas & Propagation*, Vol. 5, No. 3, 305–315, 2011.

[14] Salucci, M., G. Gottardi, N. Anselmi, and G. Oliveri, "Planar thinned array design by hybrid analytical-stochastic optimisation," *IET Microwaves, Antennas & Propagation*, Vol. 11, No. 13, 1841–1845, Oct. 2017.

[15] Keizer, W. P. M. N., "Linear array thinning using iterative FFT techniques," *IEEE Transactions on Antennas and Propagation*, Vol. 56, No. 8, 2757–2760, Aug. 2008.

[16] Gu, L., Y.-W. Zhao, Z.-P. Zhang, L.-F. Wu, Q.-M. Cai, and J. Hu, "Linear array thinning using probability density tapering approach," *IEEE Antennas and Wireless Propagation Letters*, Vol. 18, No. 9, 1936–1940, Sep. 2019.

[17] Zhou, Z., C. Zeng, and B. Chen, "Fast low-sidelobe pattern synthesis for linear array thinning utilizing a modified iterative Chirp-Z transform technique," *IEEE Sensors Journal*, Vol. 21, No. 20, 23 480–23 491, Oct. 2021.

[18] Dai, D., M. Yao, H. Ma, W. Jin, and F. Zhang, "An asymmetric mapping method for the synthesis of sparse planar arrays," *IEEE Antennas and Wireless Propagation Letters*, Vol. 17, No. 1, 70–

73, Jan. 2018.

[19] Wen, H., P.-F. Gu, Z. He, N. Yang, K. W. Leung, J.-X. Wang, Z.-H. Fan, and D.-Z. Ding, "A three-step mapping method for the synthesis of sparse planar arrays," *IEEE Transactions on Antennas and Propagation*, Vol. 73, No. 3, 1712–1724, Mar. 2025.

[20] Gong, Y., S. Xiao, Y. Zheng, and B. Wang, "Synthesis of multiple-pattern planar arrays by the multitask Bayesian compressive sensing," *IEEE Antennas and Wireless Propagation Letters*, Vol. 20, No. 8, 1587–1591, Aug. 2021.

[21] Kedar, A., P. Vangol, and A. Mahesh, "Hybridization of bayesian compressive sensing and array dilation technique for synthesis of linear isophoric sparse antenna arrays," *IEEE Transactions on Antennas and Propagation*, Vol. 71, No. 5, 4066–4074, May 2023.